

## Electronic Supplementary Information (EIS)

### **Highly Stable Chiral Bimetallic Mesoporous Platinum-Ruthenium Electrodes for Enantioselective Recognition**

Sopon Butcha,<sup>\*a</sup> Natthaphong Kaewwan,<sup>b</sup> Krissanapat Yomthong,<sup>b</sup> Zikkawas Pasom,<sup>b,c</sup> Alexander Kuhn<sup>b,c</sup> and Chularat Wattanakit<sup>b</sup>

---

<sup>a</sup>Department of Chemistry, Faculty of Science and Technology, Thammasat University, 12120, Pathum Thani, Thailand. E-mail: [soponb22@tu.ac.th](mailto:soponb22@tu.ac.th)

<sup>b</sup>School of Energy Science and Engineering, Vidyasirimedhi Institute of Science and Technology, 21210, Rayong, Thailand.

<sup>c</sup>University of Bordeaux, CNRS UMR 5255, Bordeaux INP, Site ENSCBP, 33607, Pessac, France.

**DOI: 10.1039/x0xx00000x**

---

## Table of Contents

Contents	Pages
Experimental procedures	3
Chemicals	3
Synthesis of chiral-imprinted bimetallic mesoporous Pt-Ru electrodes	3
Characterization of chiral-imprinted bimetallic mesoporous Pt-Ru electrodes	3
Enantioselective recognition of MA on chiral-imprinted bimetallic mesoporous Pt-Ru electrodes	3
Results and Discussion	4
Effect of deposition potential	4
Fig. S1 Top-view FE-SEM images of mesoporous Pt-Ru electrodes obtained for different deposition potentials	4
Fig. S2 FE-SEM/EDS analysis of the Pt-Ru bimetallic electrode prepared with different deposition potentials	4
Fig. S3 Cyclic voltammograms of the Pt-Ru bimetallic electrodes prepared with different deposition potentials	5
Fig. S4 Cross-sectional FE-SEM images of Pt-Ru films prepared with various deposition charge densities	5
Fig. S5 Effect of Pt-Ru ratio in the plating mixture on the electrooxidation efficiency of R-MA	6
Fig. S6 Structural analysis of bimetallic Pt-Ru electrodes	6
Fig. S7 Surface analysis of bimetallic Pt-Ru electrodes	7
Fig. S8 Differential pulse voltammograms (DPVs) of non-imprinted (N-imp) Pt-Ru electrodes	7
Fig. S9 Differential pulse voltammograms (DPVs) of the electrooxidation of MA with various (R)-MA imprinted Pt-Ru electrodes	7
Fig. S10 Differential pulse voltammograms (DPVs) of the electrooxidation of MA with various (S)-MA imprinted Pt-Ru electrodes	8
Scheme. S1 Proposed mechanisms for the electrooxidation of mandelic acid via a two or four electron transfer	8
Table. S1 Elemental analysis of the surface of Pt-Ru electrodes by EDS-SEM	8
Table. S2 The d-spacing information measured by XRD	8
Table. S3 Relative peak areas of the different chiral recognition experiments with chiral imprinted electrodes extracted from DPVs	9
References	9

## Experimental Procedures

### Chemicals

R-mandelic acid ((R)-MA), S-mandelic acid ((S)-MA), hexachloroplatinic acid hydrate ( $\text{H}_2\text{PtCl}_6 \cdot x\text{H}_2\text{O}$ ), ruthenium(III) chloride hydrate ( $\text{RuCl}_3 \cdot x\text{H}_2\text{O}$ ), and polyoxyethylene (20) cetyl ether ( $\text{HO}(\text{CH}_2\text{CH}_2\text{O})_{20}\text{C}_{16}\text{H}_{33}$ , Brij<sup>®</sup> 58) were received from Sigma-Aldrich. Hydrochloric acid (HCl) and sulfuric acid ( $\text{H}_2\text{SO}_4$ ) were obtained from Alfa. MilliQ water ( $18.2 \text{ M}\Omega \cdot \text{cm}$  at  $25^\circ\text{C}$ ) was employed for all experiments. All chemicals were used without further purification.

### Synthesis of chiral-imprinted bimetallic mesoporous Pt-Ru electrodes

First, the electroplating mixture was prepared by mixing the metal salts (29 wt%), including 0.1656 g of  $\text{H}_2\text{PtCl}_6 \cdot x\text{H}_2\text{O}$  and 0.0844 g of  $\text{RuCl}_3 \cdot x\text{H}_2\text{O}$  (40 Pt: 60 Ru at%), and 0.3625 g of Brij<sup>®</sup> 58 (42 wt%). Then, the mixture was heated at  $80^\circ\text{C}$  until the metal salts were homogeneously mixed with the non-ionic surfactant. At the same time, 0.0125 g of (S)-MA or (R)-MA (0.05 weight ratio of MA/metal salts), acting as a chiral template, was dissolved in 0.25 g of MilliQ water (29 wt%). Then, the MA solution was added to the electroplating gel. The gel was mixed vigorously, sealed in a vial, and subjected to three heating/cooling cycles between  $40^\circ\text{C}$  for 45 min with constant heating and at  $25^\circ\text{C}$  for 15 min. Finally, the electroplating gel was allowed to equilibrate at  $40^\circ\text{C}$  before use. In the case of the non-imprinted mesoporous Pt-Ru electrodes, the preparation method was repeated as mentioned above, excluding the addition of MA template to the plating gel.

For electrodeposition, the plating gel was put on a gold-coated glass slide as a substrate. The electrochemical deposition was carried out with a three-electrode configuration using Ag/AgCl (sat. KCl), a Pt mesh (geometric area of  $1 \text{ cm}^2$ ), and the gold-coated glass slide (geometric area of  $0.25 \text{ cm}^2$ ) as a reference, counter and working electrodes, respectively, connected to a potentiostat (Metrohm  $\mu\text{Autolab}$  Type III). All recordings were analyzed using the Nova (version 2.0) software. Electrodeposition of the Pt-Ru electrodes was performed at  $40^\circ\text{C}$  at  $-0.20$ ,  $-0.15$ , and  $-0.10 \text{ V}$  (Ag/AgCl) with injected deposition charge densities of 1, 2, 4, 6, and 8  $\text{C cm}^{-2}$ .

### Characterization of chiral-imprinted bimetallic mesoporous Pt-Ru electrodes

The Pt-Ru electrodes were physically and electrochemically characterized by several techniques. To determine the electrochemically active area, cyclic voltammetry (CV) was performed in  $0.5 \text{ M H}_2\text{SO}_4$  at a scan rate of  $100 \text{ mV s}^{-1}$  until identical voltammograms were obtained. The surface morphology (both top-view and cross-sectional imaging) and the composition and dispersion of the elements of the Pt-Ru electrodes were monitored by Field Emission Scanning Electron Microscopy (FE-SEM) equipped with an Energy Dispersive X-ray spectrometry (FE-SEM/EDS) on a JEOL, JSM-7610F. Porosity of the ultra-thin Pt-Ru layers was examined by Transmission Electron Microscopy (TEM) with a JEOL JEM-ARM200F microscope at  $200 \text{ kV}$ . The alloy structure of Pt-Ru was determined by X-ray diffraction (XRD) on a Bruker D8 ADVANCE instrument with  $\text{Cu K}\alpha$  radiation at  $40 \text{ kV}$  and  $40 \text{ mA}$  using a thin-film analysis mode. The metallic state of the Pt-Ru was determined by X-ray Photoelectron Spectroscopy (XPS) performed on a JEOL JPS-9010 equipped with a monochromatic  $\text{Al K}\alpha$  source. Prior to analysis, Pt-Ru samples were pretreated with a low-energy electron flood gun. The  $\text{C } 1s$  peak at  $284.7 \text{ eV}$  was used as a reference to correct the positions of the other spectra. The depth profile analysis of XPS was carried out by etching the Pt-Ru films with an argon ion gun for 5 s at an etching rate of approximately  $2.50 \text{ nm s}^{-1}$ , meaning that the total removed sample layer was around 14 nm. Furthermore, elemental analysis by XPS was calculated using the relative integrated peak areas of the Pt  $4f$  and Ru  $3d$  and reported in atomic percentages (at%) unit.

### Stability testing of chiral-imprinted bimetallic mesoporous Pt-Ru electrodes via enantioselective recognition

Chiral recognition was examined using (S)-MA or (R)-MA imprinted mesoporous Pt-Ru electrodes, produced with a deposition charge density of  $4 \text{ C cm}^{-2}$ . The study was carried out by Differential Pulsed Voltammetry (DPV) with the following parameters: step potential of  $0.1 \text{ V}$ , modulation amplitude of  $0.05 \text{ V}$ , modulation time of  $0.5 \text{ s}$ , interval time of  $0.5 \text{ s}$ , and a solution of  $10 \text{ mM}$  mandelic acid in  $10 \text{ mM HCl}$  as supporting electrolyte ( $\text{pH } 1.4$ ). Before analysis, the solution was degassed by nitrogen bubbling for 30 min. The electrode potential was scanned from  $0.2$  to  $0.8 \text{ V}$ . CV scans in a  $0.5 \text{ M H}_2\text{SO}_4$  solution with a scan rate of  $100 \text{ mV s}^{-1}$  were performed after the analysis to eliminate chiral information.

Enantioselectivity between (R)-MA and (S)-MA was calculated with the following the relationship

$$\text{Enantioselectivity} = \frac{A_S}{A_R} \quad \text{or} \quad \frac{A_R}{A_S} \quad (1)$$

with  $A_S$  and  $A_R$  being peak areas of either (R)-MA or (S)-MA DPVs integrated by OriginPro version 8.5.

## Results and Discussion

### Effect of deposition potentials

During the co-electrodeposition, the applied reduction potentials were varied from -0.20 to -0.15 and -0.10 V (vs. Ag/AgCl). FE-SEM images as shown in **Fig. S1** illustrate rough external surfaces with attached nanoparticles in the cases of highly negative potentials (-0.20 and -0.15 V), while applying -0.1 V leads to a smooth external surface. The distribution of Pt and Ru elements in the Pt-Ru films was analyzed by the FE-SEM/EDS (**Fig. S2**) and summarized in **Table. S1**. Applying different potentials results in a non-significant distribution of Pt and Ru elements of about 50 Pt:50 Ru at% in the deposited films. The elemental ratio of approximately 50 Pt:50 Ru at% improves the electrooxidation of alcohol compounds since Ru can supply oxygen atoms to the active Pt and the Ru itself has a carbon monoxide tolerance that can improve the electrochemical catalyst stability. [1]

The Pt-Ru layers were electrochemically characterized by cyclic voltammetry (CV) in a 0.5 M H<sub>2</sub>SO<sub>4</sub> solution at a scan rate of 100 mV s<sup>-1</sup>. Rough external surfaces of Pt-Ru can also be confirmed by cyclic voltammograms shown in **Fig. S3**. The CV curves reveal larger signals for more negative deposition potentials, implying a higher active surface area due to the rough outermost surface. The rough external surface of mesoporous metal films can introduce non-selective sites for electrochemical reactions, because the selective sites are located in the cavities of the mesopores. [19, 20] In order to decrease the influence of these unfavourable reaction sites, mesoporous Pt-Ru electrodes were generated at -0.10 V for further studies.

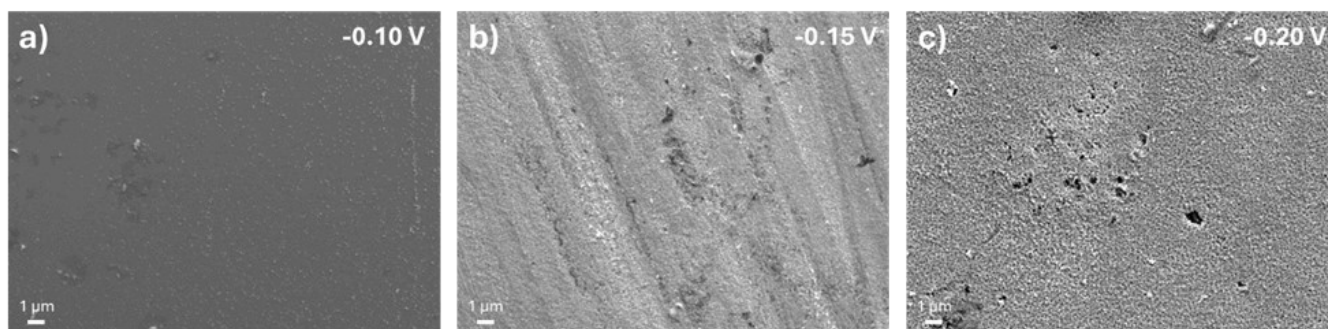


**Fig. S1** Top-view FE-SEM images of mesoporous Pt-Ru electrodes obtained for different deposition potentials: a) -0.10 V, b) -0.15 V, and c) -0.20 V (vs. Ag/AgCl) with a controlled injected charge density of 4 C cm<sup>-2</sup> (scale bar 1 µm).

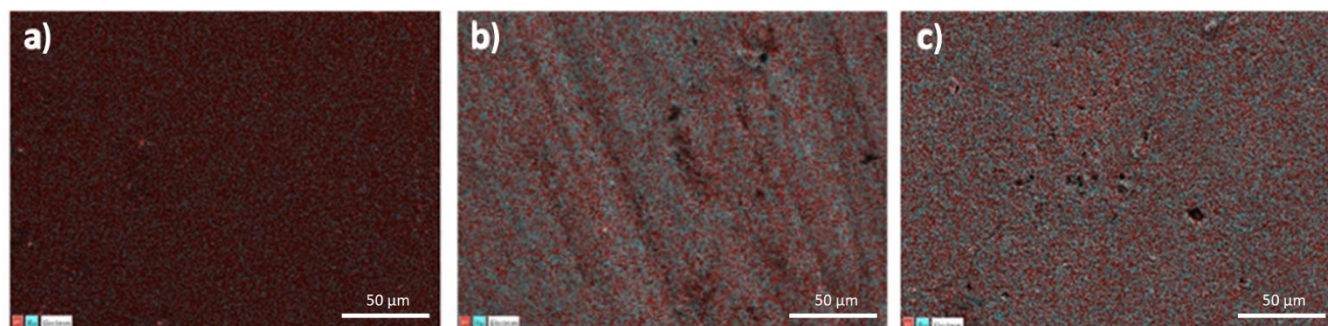


**Fig. S2** FE-SEM/EDS analysis of the bimetallic Pt-Ru electrode prepared with different deposition potentials: a) -0.10 V, b) -0.15 V, and c) -0.20 V (vs. Ag/AgCl) with a controlled injected charge density of 4 C cm<sup>-2</sup> (scale bar 50 µm, red and light blue colors represent Pt and Ru respectively).

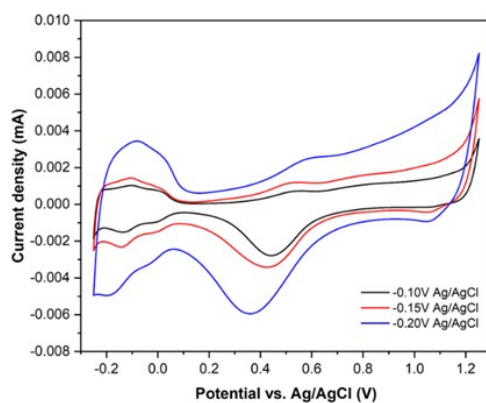


**Fig. S3** Cyclic voltammograms of the bimetallic Pt-Ru electrodes prepared with different deposition potentials of -0.10 V (black), -0.15 V (blue), and -0.20 V (red) with an injected charge density of  $4 \text{ C cm}^{-2}$ . All data were obtained after 15 CV scans in  $0.5 \text{ M H}_2\text{SO}_4$  at a scan rate of  $100 \text{ mV s}^{-1}$ .

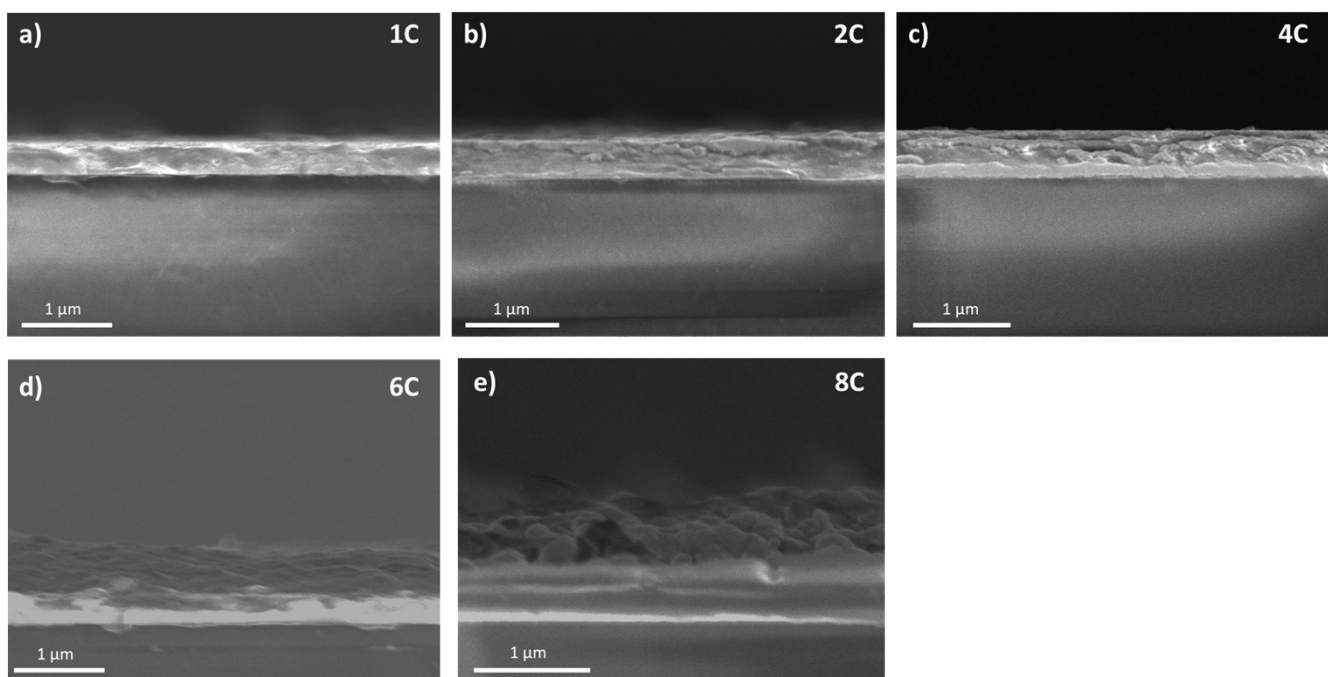


**Fig. S4** Cross-sectional FE-SEM images of Pt-Ru films prepared with various injected charge densities: a) – e) Pt-Ru electrodes prepared with charge densities of 1, 2, 4, 6 and  $8 \text{ C cm}^{-2}$  at a deposition potential of -0.1 V.

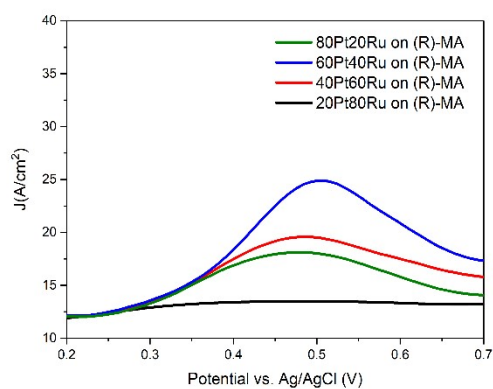


**Fig. S5** Effect of Pt-Ru ratio in the plating mixture on the electrooxidation efficiency of R-MA.

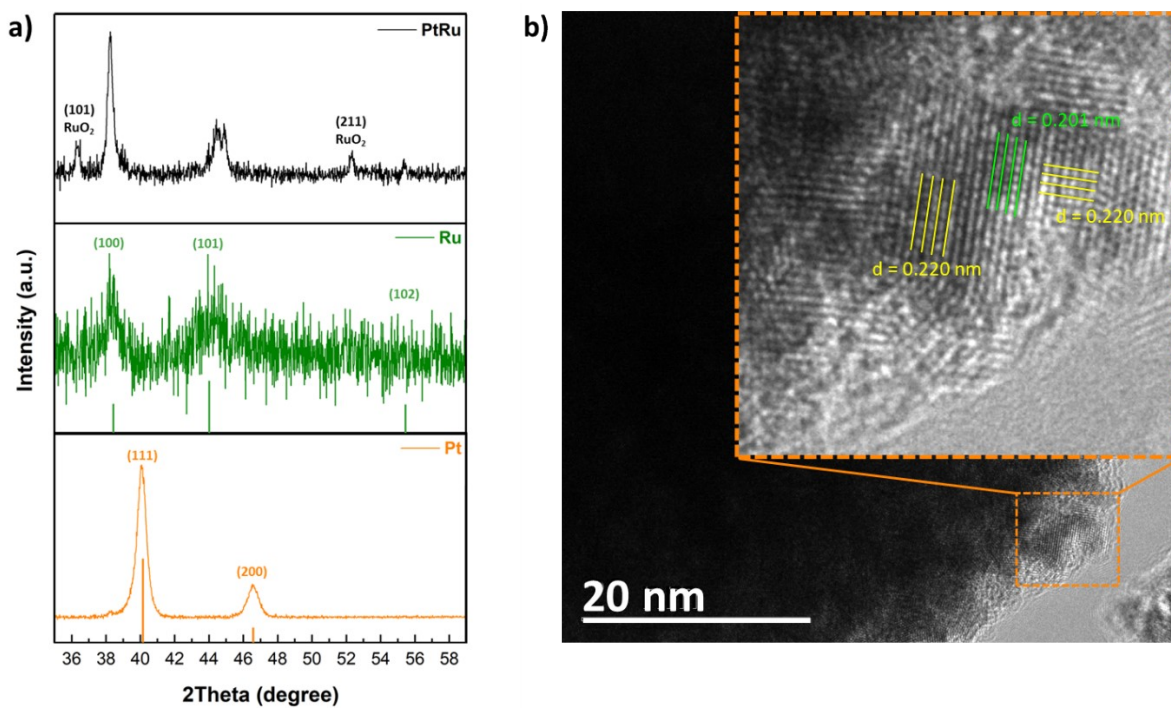


**Fig. S6** Structural analysis of bimetallic Pt-Ru electrodes: a) XRD pattern of Pt, Ru and Pt-Ru films, and b) HR-TEM image of an ultra-thin Pt-Ru film.

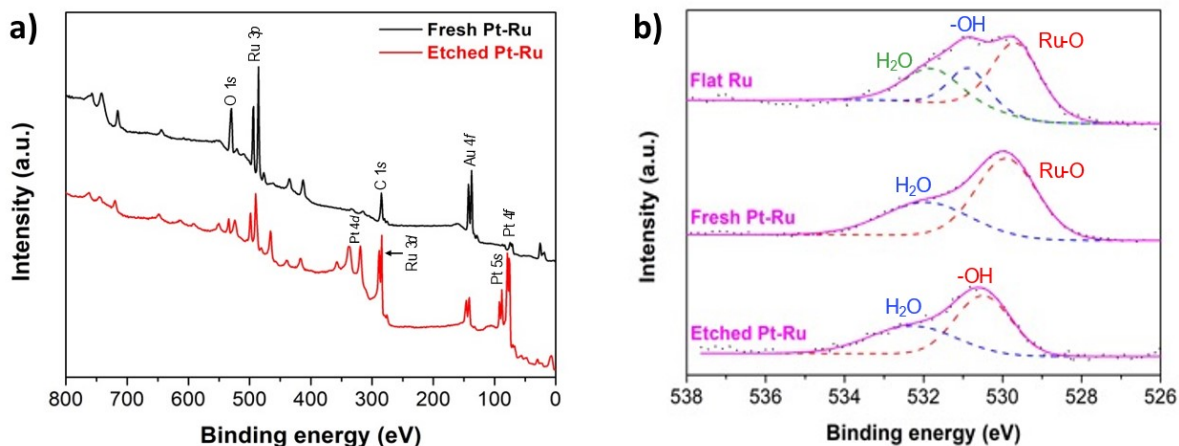


**Fig. S7 Surface analysis of bimetallic Pt-Ru electrodes:** a) Wide scan XPS spectra of fresh and etched Pt-Ru electrodes, and b) Narrow scan XPS spectra of flat Ru, as well as fresh and etched Pt-Ru electrodes in the region of O 1s.

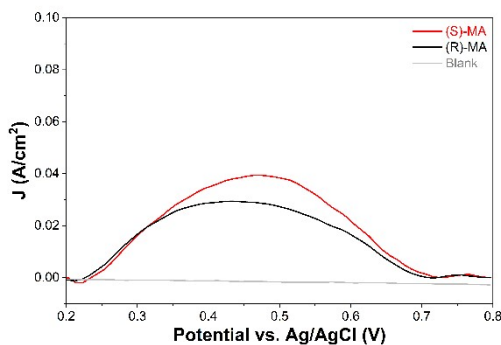


**Fig. S8 Differential pulse voltammograms (DPVs) of the non-imprinted (N-imp) Pt-Ru electrodes.** The experiments were conducted in 10 mM (R)-MA (black) and (S)-MA (red) dissolved in 10 mM HCl supporting (dash line, blank) electrolyte solution. All DPVs were plotted through the background correction. The enantioselectivity is approximately  $0.9 \pm 0.2$ .

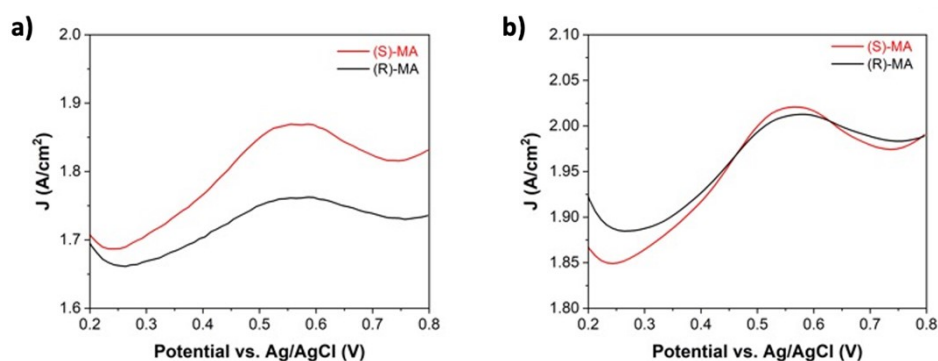


**Fig. S9 Differential pulse voltammograms (DPVs) of the electrooxidation of MA with various (S)-MA imprinted (S-imp) Pt-Ru electrodes:** a) and b) S-imp Pt-Ru electrodes after erasing chirality for 20 and 30 cycles, respectively. The experiments were performed in 10 mM (R)-MA (black) and (S)-MA (red) dissolved in 10 mM HCl supporting electrolyte solution. Erasing chiral information was achieved by CV scan from -0.25 to +1.40 V performed in 0.5 M  $\text{H}_2\text{SO}_4$  solution at a scan rate of  $100 \text{ mV s}^{-1}$ .

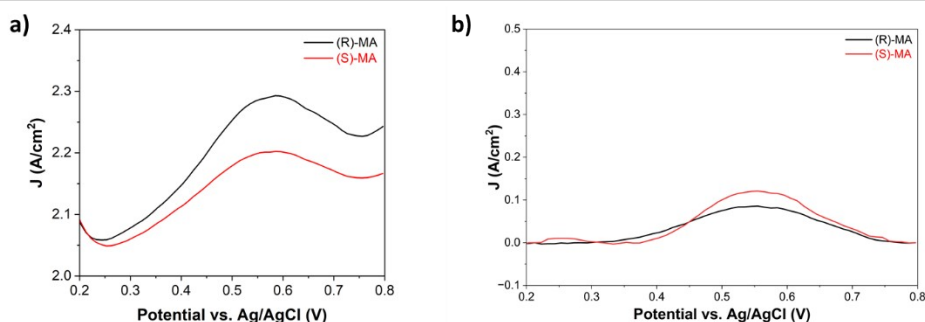
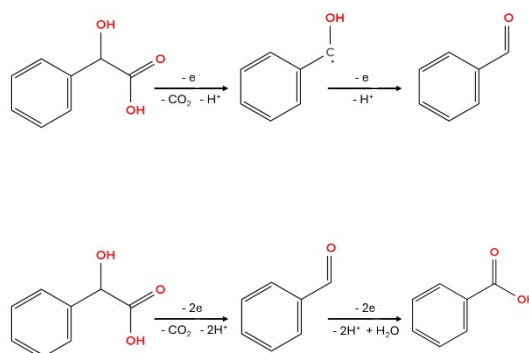


**Fig. S10** Differential pulse voltammograms (DPVs) of the electrooxidation of MA with various (R)-MA imprinted (R-imp) Pt-Ru electrodes: a) and b) R-imp Pt-Ru electrodes after erasing chirality for 20 and 30 cycles, respectively. The experiments were conducted in 10 mM (R)-MA (black) and (S)-MA (red) dissolved in 10 mM HCl supporting electrolyte solution. Erasing the chiral information was achieved by CV scan from -0.25 to +1.40 V performed in 0.5 M H<sub>2</sub>SO<sub>4</sub> solution at a scan rate of 100 mV s<sup>-1</sup>.



**Scheme. S1** Proposed mechanisms for the electrooxidation of mandelic acid via a two or four electron transfer. The figure was adapted from Ref. [2]

**Table. S1** Elemental analysis on the surface of Pt-Ru electrodes obtained by EDS-SEM.

Applied Potentials (V vs. Ag/AgCl)	Pt (at %)	Ru (at %)
-0.20	45	55
-0.15	44	54
-0.10	50	50

**Table. S2** The d-spacing information obtained by XRD.

2Theta (degree)	(hkl)	d-spacing (nm)
38.2	Ru (100)	0.235
44.0	Ru (101)	0.210
40.1	Pt (111)	0.225
46.5	Pt (200)	0.195
38.3	Pt-Ru	0.235
44.3	Pt-Ru	0.204

**Table. S3** Relative peak areas of the different chiral recognition experiments with chiral imprinted electrodes extracted from DPVs. Peak areas of either (R)-MA or (S)-MA electrooxidation were integrated with OriginPro version 8.5.

Electrodes	Relative peak areas	
	(R)-MA/(S)-MA	(S)-MA/(R)-MA
(R)-MA Pt	2.5 ± 0.1	-
Erased (R)-MA Pt after 10 cycles	1.0 ± 0.1	-
(R)-MA Pt-Ru	7.1 ± 0.1	-
Erased (R)-MA Pt-Ru after 10 cycles	2.4 ± 0.7	-
Erased (R)-MA Pt-Ru after 20 cycles	1.2 ± 0.1	-
Erased (R)-MA Pt-Ru after 30 cycles	1.0 ± 0.2	-
(S)-MA Pt-Ru	-	6.0 ± 1.0
Erased (S)-MA Pt-Ru after 10 cycles	-	2.7 ± 0.2
Erased (S)-MA Pt-Ru after 20 cycles	--	1.7 ± 0.1
Erased (S)-MA Pt-Ru after 30 cycles		1.1 ± 0.1

## References

- 1 E. A. Paoli, F. Masini, R. Frydendal, D. Deiana, C. Schlaup, M. Malizia, T. W. Hansen, S. Horch, I. E. L. Stephens and I. Chorkendorff, *Chem. Sci.*, 2015, **6**, 190-196.
- 2 M. Borazjani, A. Mehdinia, A. Jabbari, *J. Electroanal. Chem.*, 2017, **805**, 83-90.